JOURNAL OF VIROLOGY, May 2006, p. 4344–4355 Vol. 80, No. 9
0022-538X/06/$08.00+0 doi:10.1128/JVI.80.9.4344–4355.2006

Identification of Functionally Important Negatively Charged Residues in the Carboxy End of Mouse Hepatitis Coronavirus A59 Nucleocapsid Protein

Sandhya Verma,[1] Valerie Bednar,[2] Andrew Blount,[2] and Brenda G. Hogue[1]*

School of Life Sciences and The Biodesign Institute[1] and Barrett Honors College,[2] Arizona State University, Tempe, Arizona 85287

Received 2 August 2005/Accepted 3 February 2006

The coronavirus nucleocapsid (N) protein is a multifunctional viral gene product that encapsidates the RNA genome and also plays some as yet not fully defined role in viral RNA replication and/or transcription. A number of conserved negatively charged amino acids are located within domain III in the carboxy end of all coronavirus N proteins. Previous studies suggested that the negatively charged residues are involved in virus assembly by mediating interaction between the membrane (M) protein carboxy tail and nucleocapsids. To determine the importance of these negatively charged residues, a series of alanine and other charged-residue substitutions were introduced in place of those in the N gene within a mouse hepatitis coronavirus A59 infectious clone. Aspartic acid residues 440 and 441 were identified as functionally important. Viruses could not be isolated when both residues were replaced by positively charged amino acids. When either amino acid was replaced by a positively charged residue or both were changed to alanine, viruses were recovered that contained second-site changes within N, but not in the M or envelope protein. The compensatory role of the new changes was confirmed by the construction of new viruses. A few viruses were recovered that retained the D_{441}-to-arginine change and no compensatory changes. These viruses exhibited a small-plaque phenotype and produced significantly less virus. Overall, results from our analysis of a large panel of plaque-purified recovered viruses indicate that the negatively charged residues at positions 440 and 441 are key residues that appear to be involved in virus assembly.

Coronaviruses are enveloped RNA viruses that cause respiratory and enteric infections in humans and many domesticated animals. Members of the family *Coronaviridae* contain single-stranded, positive-sense genomes that range from approximately 27 to 31 kb in length. The viral genes are expressed through a discontinuous transcription mechanism that yields a nested set of subgenomic RNAs (39). Coronavirus virions contain at least three envelope proteins, membrane (M), spike (S), and envelope (E). The genomic RNA is encapsidated by the nucleocapsid (N) protein as a helical nucleocapsid (10, 26). The S protein is the viral receptor attachment protein that facilitates infection through fusion of viral and cellular membranes and is the major target of neutralizing antibodies during infection (15). The M protein is a major envelope component that plays an important role in virus assembly (11, 21, 31, 33, 46). The E protein is a minor component of the viral envelope that also plays a critical role in virus budding. Coexpression of the E and M proteins is sufficient for formation of virus-like particles (3, 8, 46). Deletion of the E gene from the mouse hepatitis coronavirus (MHV-CoV) genome results in severely crippled virus (23), whereas elimination of expression of the gene in porcine transmissible gastroenteritis coronavirus blocks virus assembly (9, 34). Recently, the severe acute respiratory syndrome coronavirus (SARS-CoV) and MHV-CoV E proteins were shown to exhibit viroporin activity (25, 27, 48). Virions assemble at intracellular membranes of the endoplasmic reticulum Golgi intermediate compartment (44).

The focus of this report is the multifunctional N protein. The protein is a major structural component of virions that plays a role in virus assembly though interactions with the viral RNA, the M protein, and N-N interactions (13, 22, 28, 30). Results from a number of studies suggest that N also plays a role in viral RNA synthesis (1, 2, 5, 7, 12, 45). Recovery of infectious cloned coronaviruses is increased when N protein transcripts are included during RNA transfection (1, 4, 49). Recent data strongly support earlier studies by providing direct evidence that N is involved in viral RNA replication and/or transcription (40). N may also be involved in the translation of viral mRNAs (42).

Coronavirus N proteins are phosphorylated. The proteins are highly basic, with isoelectric points (pI) of 10.3 to 10.7 (24). A three-domain structure for the protein has been proposed based on early sequence comparisons of MHV strains (35). The amino terminal and central domains of all coronavirus N proteins exhibit an overall positive charge, whereas the carboxy-terminal domain is acidic. Conservation of negatively charged amino acids within the carboxy ends of all coronavirus N proteins suggests that the residues are functionally relevant. Furthermore, data from an earlier study suggest that the carboxyl end of the protein mediates interaction with the M protein during assembly, and the charged resides within the region were hypothesized to possibly facilitate the interaction (22).

Within the carboxy-terminal 22 amino acids of the MHV-CoV N protein there are eight negatively charged residues (Fig. 1). We therefore considered whether the charges are important for virus viability and output. The rationale for fo-

* Corresponding author. Mailing address: The Biodesign Institute, P.O. Box 875401, Arizona State University, Tempe, AZ 85287-5401. Phone: (480) 965-9478. Fax: (480) 727-7615. E-mail: Brenda.Hogue@asu.edu.

```
              +   -++-- -     + +    +   +-   --+       --    -  ---
MHV           RQAQEKKDEVDNVSVAKPKSSVQRNVSRELTPEDRSLLAQILDDGVVPDGLEDDSNV 454
OC43          RGHKNGQGENDNISVAVPKSRVQQNKSRELTAEDISLLKKMDEP-----YTEDTSEI 448
BCV           RGQKNGQGENDNISVAAPKSRVQQNKSRELTAEDISLLKKMDEP-----YTEDTSEI 448
              -      + ++          - --  +          -
SARS          EAQPLPQRQKKQPTVTLLPAADMDDFSRQLQNSMSGASADSTQA              422
```

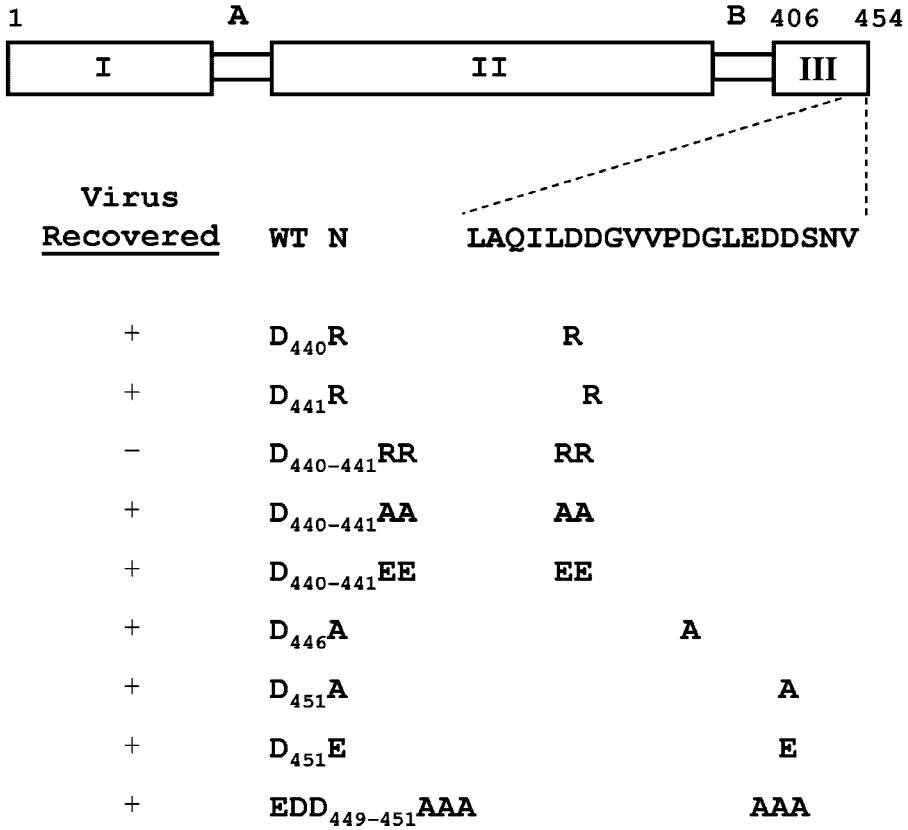

FIG. 1. Schematic illustration of N negatively charged mutant constructs. An alignment of the negatively charged region in the carboxy ends of the N proteins of representative group II coronaviruses (MHV-CoV A59 [MHV], human coronavirus OC43, and bovine coronavirus [BCV]) and the newest member of the family, SARS-CoV (SARS), was generated using ClustalW (43). Terminal amino acid numbers are shown at the end of each sequence. Positively and negatively charged amino acid residues are indicated above the MHV and SARS sequences by plus and minus signs, respectively. A schematic of the three-domain model of the coronavirus N protein separated by the A and B spacer domains (35) is shown, with the carboxy-terminal amino acids expanded where mutations were introduced. The amino acid substitutions are indicated below the sequence of the extreme end of domain III. Recovery of mutant viruses is indicated by plus and minus signs at the left of each mutant virus designation. WT, wild type.

cusing on the residues was based on previous studies from our laboratory and others (13, 22), the conservation and concentration of the negative charges, and the fact that charged residues can play an important role in helping to mediate protein-protein interactions. Alanine and other charged-residue codon substitutions were introduced in place of the conserved negative charges in the N gene within an MHV-CoV A59 infectious clone. Results from the panel of mutant viruses identified aspartic acid residues 440 and 441 as functionally important. Maintenance of the net negative charge across the COOH end appears to drive the selection of new viruses when charge reversal substitutions are placed at these positions. These residues likely play roles in helping to mediate electrostatic interactions between N and other proteins, most likely the M protein, during virus assembly, but they may also contribute to other protein interactions that are important for the other functions of N.

MATERIALS AND METHODS

Cells and viruses. Stocks of wild-type MHV-CoV A59 and infectious cloned viruses were grown in mouse 17 clone 1 (17Cl1) cells. Titers were determined in mouse L2 cells. L2 and 17Cl1 cells were maintained in Dulbecco's modified Eagle's medium (DMEM) supplemented with 5 to 10% heat-inactivated fetal calf serum, as previously described (41). Baby hamster kidney (BHK) cells expressing the MHV Bgp1a receptor were kindly provided by Ralph Baric, University of North Carolina at Chapel Hill (50). The cells were maintained on Glasgow modified Eagle's medium supplemented with 5% heat-inactivated fetal calf serum, 10% tryptose phosphate broth, glutamine, penicillin-streptomycin, and 80 μg/ml Geneticin (G418).

TABLE 1. Oligonucleotides used in this study

Name	Primer sequence[a]	Use
$D_{440}R$	CAC TAC GCC ATC **ACG** AAG GAT CTG AGC CAA CAG	Mutagenesis
$D_{441}R$	CAC TAC GCC **ACG** ATC AAG GAT CTG AGC CAA CAG	Mutagenesis
$D_{440-441}RR$	CAC TAC GCC **ACG** **ACG** AAG GAT CTG AGC CAA CAG	Mutagenesis
$D_{440-441}AA$	CAC TAC GCC **AGC** **AGC** AAG GAT CTG AGC CAA CAG	Mutagenesis
$D_{440-441}EE$	CAC TAC GCC **CTC** **CTC** AAG GAT CTG AGC CAA CAG	Mutagenesis
$D_{446}A$	CGT AGT GCC A**GC** **T**GG GTT AGA AG	Mutagenesis
$D_{451}A$	CAC ATT AGA **GGC** ATC TTC TAA CCC ATC TGG CAC	Mutagenesis
$D_{451}E$	CAC ATT AGA **CTC** ATC TTC TAA CCC ATC TGG CAC	Mutagenesis
$EDD_{449-451}AAA$	CAC ATT AGA **GGC** **AGC** **TGC** TAA CCC ATC TGG CAC	Mutagenesis
$R_{425}G$ Forward	GCT CTG TGC AGC GAA ATG TAA GT**G** **GC**G AAT TAA CCC C	Mutagenesis top stand
$R_{425}G$ Reverse	CAG ACT TCT ATC CTC TGG GGT TAA TTC **GCC** ACT TAC ATT TCG C	Mutagenesis bottom strand
$T_{428}ND_{440}R$ Forward	GCA GCG AAA TGT AAG TAG AGA ATT A**AA** **C**CC AGA GGA TAG AAG	Mutagenesis top strand
$T_{428}ND_{440}R$ Reverse	GAG CCA ACA GAC TTC TAT CCT CTG G**GT** **T**TA ATT CTC TAC TTA C	Mutagenesis bottom strand
$A_{436}DD_{441}R$ Forward	AAC CCC AGA GGA TAG AAG TCT GTT G**GA** **C**CA GAT CCT TGA T**CG** **T**G	Mutagenesis top strand
$A_{436}DD_{441}R$ Reverse	CAC TAC GCC **ACG** ATC AAG GAT CTG **GTC** CAA CAG AC	Mutagenesis bottom strand
MHV M Reverse	CGG TAC CTT TCA TAT CTA TAC	Sequencing of E gene
MHV 4 Reverse	AGT CTG CTT TGG CTG ATT CCT TC	Sequencing of M gene
MHV 6 Reverse	TTC CTG AGC CTG TCT ACG	Sequencing of M gene
MHV 7 Forward	ATT CTG GTG GTG CTG ATG AAC CGG C	Sequencing of N gene
MHV 8 Forward	GGC AGA AGC TCC TCT GTA AAC C	Sequencing of N gene
MHV EM (+)	CAG AAC TGT CCA ACA GGC CGT TAG CAA G	RT-PCR (+) strands
MHV EM (−)	GCA ACC CAG AAG ACA CCT TCA ATG C	RT-PCR (−) strands
MHV MN (+)	CCA CCT CTA CAT GCA AGG TGT TAA GC	RT-PCR (+) strands
MHV MN (−)	GGT CTG CCA CAA CCT TCT CTA TCT	RT-PCR (−) strands

[a] Mutagenized codons are boldface and underlined.

Construction of amino acid substitution mutants. Plasmid pGEM-5Zf(−)M-N, a pGEM-5Zf(−) vector (Promega) containing the entire M and N genes (EcoRV-SacI fragment), was used as the template for mutagenesis of the N gene. The oligonucleotides used to perform site-directed mutagenesis are listed in Table 1. The original mutants were constructed using the GeneEditor site-directed mutagenesis system (Promega), basically according to the manufacturer's instructions. The four reconstructed N double mutants were constructed by whole-plasmid PCR using *Pfu* polymerase (Stratagene) in the pGEM-5zf(−)M-N background, which contained the previously modified $D_{440}R$ or $D_{441}R$ mutation. Following an initial incubation at 95°C for 3 min, the following conditions were applied for 18 cycles: 95°C for 15 s, 74°C for 60 s, and 68°C for 12 min. The PCR products were incubated at 37°C for 2 h with DpnI to destroy methylated template DNA before transformation into *Escherichia coli* DH5α. The entire EcoRV-SacI region of the N gene was confirmed by sequencing. Following confirmation of the mutations in pGEM-5Zf(−)M-N, the N gene was subcloned into the MHV G clone using NheI and SacI restriction sites.

Generation of mutant viruses. Mutant viruses were generated using the MHV-CoV A59 infectious clone kindly provided by Ralph Baric, University of North Carolina at Chapel Hill (50). Full-length cDNA clones were assembled as previously described with a few modifications. Plasmids containing the cDNA cassettes spanning the MHV genome were purified using QIAfilter Maxi cartridges (QIAGEN) and digested with MluI and Esp3I for fragment A; BglI and Esp3I for fragments B and C; Esp3I for fragments D, E, and F; and SfiI and Esp3I for fragment G. The fragments were gel purified and ligated overnight in a reaction volume of 100 to 200 μl. The ligated DNA products were extracted with phenol-chloroform and ethanol precipitated. RNA transcripts were made using the mMessage mMachine T7 Transcription reagents and protocol (Ambion). Transcription reactions were carried out at 37°C for 2 h in the presence of an additional GTP. The MHV nucleocapsid gene was transcribed from pMHV-A59 N (6) using T7 RNA polymerase. N gene transcripts were polyadenylated using Ambion's poly(A) tailing system.

Full-length MHV infectious-clone and N transcripts were electroporated into BHK cells stably expressing the MHV receptor (BHK-MHVR cells). BHK-MHVR cells had been seeded the previous day to reach approximately 70% confluence for electroporation. Cells were trypsinized, washed with phosphate-buffered saline, and resuspended at a concentration of 10^7 cells/ml in OptiMEM (Invitrogen). RNA transcripts were electroporated into 800 μl of the cell suspension in a 4-mm-gap cuvette with three electrical pulses of 850 V at 25 μF using a Bio-Rad Gene Pulser II electroporator. Transfected cells were seeded in 75-cm^2 flask and incubated at 37°C. The cells were monitored for syncytia. The medium and cells were harvested 24 to 48 h after electroporation.

An aliquot of the frozen stock from the electroporated cells was used to infect L2 cells. The media were harvested from the infected cells at approximately 24 h p.i. Total RNA was extracted from cells that remained adhered to the flasks using Ambion's RNAqueous-4PCR extraction system. The extracted RNA was treated with DNase I for 15 min at 37°C. RNA was reverse transcribed using Invitrogen's Superscript reverse transcription (RT)-PCR and recommended protocol. The initial reaction mixture was incubated at 42°C for 2 min prior to reverse transcription for 50 min. The reactions were terminated by incubation at 70°C for 15 min. Template RNA was destroyed by additional incubation for 20 min at 37°C after the addition of RNase H. The RT product was subjected to 30 cycles of PCR amplification using Ambion's SuperTaq Plus. Following an initial incubation of 95°C for 5 min, the following conditions were applied: 95°C for 30 s, 59°C for 30 s, and 72°C for 90 s, followed by a final 10-min extension at 72°C. PCR products were cleaned up using QIAGEN's MiniElute columns and sequenced directly.

Ten to 20 plaques were subsequently isolated from the electroporated cell/medium virus stock. The plaques were passaged onto L2 cells. RNA was extracted from the infected cells at approximately 24 h p.i. RT-PCR was performed, and the entire E, M, and N genes were sequenced. Selected plaques were amplified on L2 cells through five passages, at which time the sequences of the E, M, and N genes were again confirmed.

Growth kinetics. Growth kinetics experiments were carried out in 17Cl1 cells infected with P5 virus stocks at a multiplicity of infection (MOI) of 5 or 1. Cell culture supernatants were collected at various times after infection. Titers were determined by plaque assay on L2 cells. At approximately 48 h p.i., the agarose/medium overlays were removed and the cells were fixed and stained with crystal violet.

Northern blotting. Monolayers of 70 to 80% confluent 17Cl1 cells in 60-mm-diameter dishes were individually infected with wild-type MHV and selected mutant viruses at an MOI of 0.1. RNA was extracted at 8 and 12 h p.i. with TRIzol (Invitrogen) according to the manufacturer's instructions. The RNA pellets were resuspended in RNase-free water. Equivalent amounts of total intracellular RNA were denatured and separated on 1% agarose gels containing formaldehyde at 85 V for 5 h essentially as described previously (41). After electrophoresis, the gels were vacuum blotted onto positively charged nylon membranes in 20× SSC (0.3 M NaCl, 0.3 M sodium citrate). Northern blotting analyses were performed using a digoxigenin-labeled 357-nucleotide MHV-CoV A59 N gene probe. The probe was transcribed using reagents for digoxigenin labeling (Roche Applied Science) according to the manufacturer's directions. Images were quantified by densitometric scanning of the fluorograms and analyzed using ImageQuant software (Molecular Dynamics).

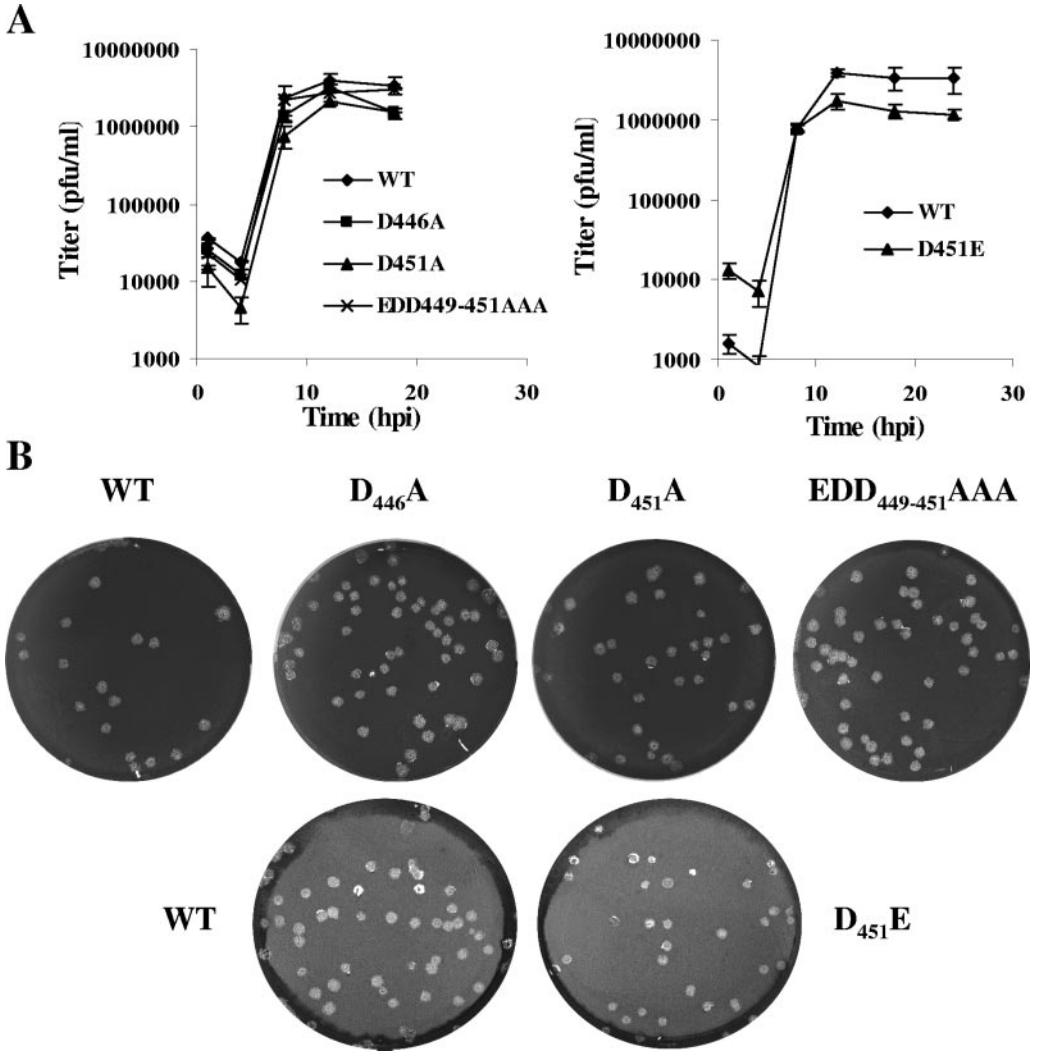

FIG. 2. Growth kinetics and plaque morphologies of $D_{446}A$, $D_{451}A$, $EDD_{449-451}AAA$, and $D_{451}E$ mutant viruses. (A) Single-step growth kinetics of mutant viruses relative to wild-type (WT) virus. Mouse 17Cl1 cells were infected with the wild-type virus and mutant viruses $D_{446}A$, $D_{451}A$, and $EDD_{449-451}AAA$ at an MOI of 5 or with wild-type and $D_{451}E$ viruses at an MOI of 1. Titers were measured by plaque assay in L2 cells at the indicated times. The error bars indicate the average deviations from the mean for two independent growth kinetic experiments. (B) Plaque sizes and morphologies of recovered mutant viruses in infected mouse L2 cells are shown.

Metabolic labeling and analysis of proteins in infected cells. Monolayers of 70 to 80% confluent 17Cl1 cells in 35-mm-diameter plates were infected with wild-type or selected mutant viruses at an MOI of 0.1 PFU/cell. At 4.5 h p.i., the cells were starved for 30 min with DMEM without methionine and cysteine prior to being labeled with 125 μCi/ml of EXPRE^{35}S^{35}S protein labeling mix (Perkin-Elmer) for 30 min. Immediately after being labeled, the cytoplasmic fraction was harvested from one set of plates. A parallel set of plates were washed and refed with DMEM containing 10 times the normal amount of methionine and cysteine and chased until 9.5 h p.i., at which time both cytoplasmic lysates and the extracellular medium fractions were harvested. The cells were washed twice with cold phosphate-buffered saline and lysed with RIPA lysis buffer (1% Triton X-100, 1% deoxycholate, 0.3% sodium dodecyl sulfate [SDS], 150 mM NaCl, 50 mM Tris-HCl, pH 7.6, 20 mM EDTA) containing 1× Complete, Mini, EDTA-free Protease Inhibitor Cocktail Tablets (Roche Applied Science). Lysates and media were clarified at 16,000 × *g* for 10 min. Virions in the extracellular media were lysed by the addition of an equal volume of 2× RIPA lysis buffer and sonication for 1.5 min at 30-s intervals with 30-s rests. Both intracellular and extracellular fractions were precleared by incubation with protein A-Sepharose at 4°C for 1 h with rocking. Viral proteins were immunoprecipitated by incubation with rabbit anti-MHV antibody F88 (K. Holmes, University of Colorado Health Sciences Center) overnight at 4°C. Immunoprecipitated protein complexes were isolated by incubation with protein A-Sepharose for 2 h at 4°C with constant rocking. The immunoprecipitates were washed five times with RIPA buffer prior to elution in SDS-polyacrylamide gel electrophoresis (PAGE) sample buffer by heating them at 95°C for 5 min and were analyzed by SDS-PAGE on 5 to 20% gradient gels. Prior to being dried, the gels were incubated for 30 min at room temperature with Amplify Fluorographic Reagent (GE Healthcare Life Sciences). Proteins were detected by fluorography. Protein products were quantified by densitometric scanning of the fluorograms and analyzed using ImageQuant software (Molecular Dynamics).

Analysis of N protein isoelectric points. Prediction of the isoelectric points of the wild-type and mutant N proteins was performed using the ScanSite pI/M_w program algorithm, with the option to include phosphorylation sites, from ExPASy's proteomics server at the Swiss Institute of Bioinformatics (http://ca.expasy.org/) (16).

RESULTS

Generation of N charged-residue mutant viruses. To begin examining the importance of the conserved negatively charged residues within the carboxy-terminal end of the MHV-CoV N

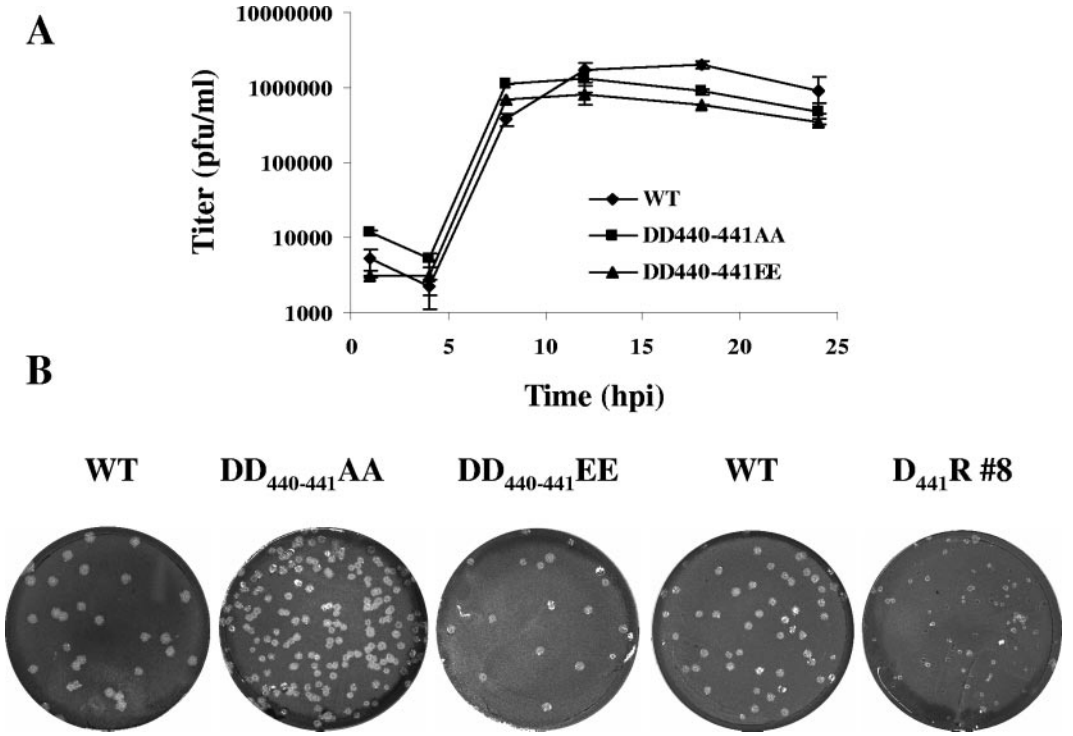

FIG. 3. Growth kinetics and plaque morphologies of $DD_{440-441}AA$, $DD_{440-441}EE$, and $D_{441}R$ no. 8 viruses. (A) Mouse 17Cl1 cells were infected with wild-type (WT), $DD_{440-441}AA$, and $DD_{440-441}EE$ viruses at an MOI of 5. Single-step growth kinetics analysis was performed by plaque assay in mouse L2 cells. The error bars indicate average deviations of two independent growth kinetics experiments. (B) Plaque sizes and morphologies of $DD_{440-441}AA$, $DD_{440-441}EE$, and $D_{441}R$ no. 8 viruses analyzed in parallel with wild-type virus in mouse L2 cells are shown.

protein, substitutions were introduced within the last 15 amino acids (Fig. 1). Negatively charged aspartic acid (D) residues at positions 440 and 441 were changed either singly to positively charged arginine (R) or doubly to R, negatively charged glutamic acid (E), or neutrally charged alanine (A). Single alanine substitutions were introduced in place of D residues at positions 446 and 451. D_{451} was also replaced by a glutamic acid residue. Additionally, a triple mutation was introduced at positions 449 to 451 in which the EDD residues were all changed to alanines. In all cases, 2 nucleotides were introduced to alter the individual amino acid codons, thus significantly decreasing the chances of reversions to allow us to study compensatory second-site changes.

All mutations were generated by site-directed mutagenesis and studied in the context of a full-length MHV-CoV A59 infectious clone (50). All full-length mutant RNAs yielded cytopathic effects characterized by centers of fusion following electroporation into BHK-MHVR cells. However, viable viruses were subsequently recovered for only eight of the nine mutants after passage onto new cells (Fig. 1). Mutant $DD_{440-441}RR$ exhibited a few centers of fusion after electroporation, but multiple attempts to passage the virus were unsuccessful. The eight viable mutant viruses were plaque purified and analyzed for their phenotypic and genetic characteristics through multiple passages. RT-PCR and sequence analysis of the N, M, and E genes before and after multiple passages were carried out to determine the genetic stability of the viruses.

Negatively charged residues 446 and 449 to 451 are not absolutely required. Analysis of the recovered viruses with alanine replacements for D_{446} and D_{451} and a triple substitution for $EDD_{449-451}$, as well as a glutamic acid substitution for residue 451, indicated that the viruses were phenotypically like the wild-type parental virus (Fig. 2). The plaque size and morphology of the viruses were indistinguishable from those of the wild type. Recovered viruses were plaque purified, and multiple plaques of each mutant were followed for five passages. Sequence analysis of P5 confirmed the stability of the introduced mutations and that no additional changes were present in the remainder of the N gene or within the E or M gene. Growth kinetics analysis demonstrated that all of the recovered viruses grew like the parental virus (Fig. 2). These results strongly suggest that the negative charges at the carboxyl end of the protein are not absolutely required for the protein to carry out its function(s).

The conserved negative charges at positions 440 and 441 are very important. The removal of the negative charges at positions D_{440} and D_{441} had a strikingly different effect on the virus, compared with the mutants described above. While centers of fusion were observed for the five mutants that encompassed these residues, only four viruses were subsequently recovered (Fig. 1). Multiple attempts to recover the $DD_{440-441}RR$ virus were not successful, indicating that the replacement of the negative charges with positive charges is detrimental to the virus. This strongly suggested that these are functionally important residues.

The apparent importance of the $DD_{440-441}$ residues was further strengthened as the recovered viruses were analyzed. First, replacement of both residues with negatively charged glutamic acid (E) yielded virus that displayed a plaque size, a

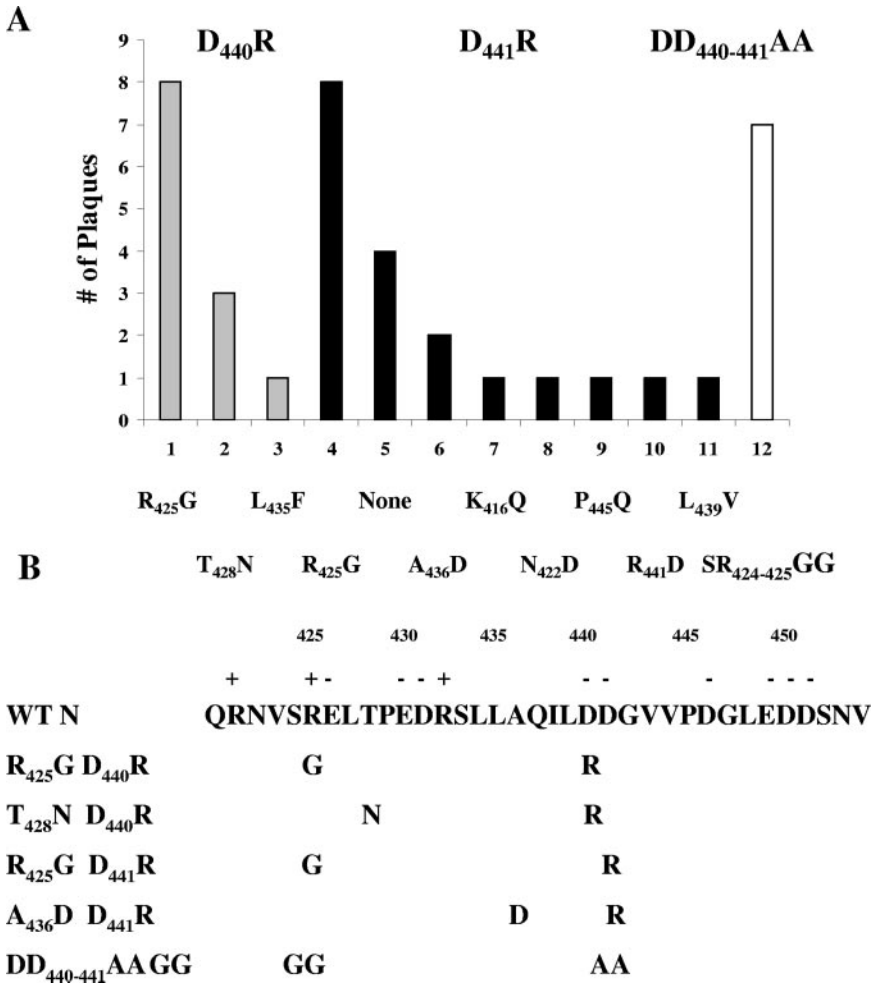

FIG. 4. Summary of sequence analysis of recovered viruses from $D_{440}R$, $D_{441}R$, and $DD_{440-441}AA$ mutants. (A) Sequence analysis of the E, M, and N genes of multiple plaques from viruses with substitutions at amino acid positions 440 and/or 441 revealed additional changes only within the N gene. The bars represent the number of plaques analyzed that exhibited the additional changes indicated below each bar. Changes are listed as the wild-type residue at each position in the N protein and the corresponding change that was identified. (B) The five additional amino acid changes identified most frequently in the $D_{440}R$, $D_{441}R$, and $DD_{440-441}AA$ mutant viruses are summarized, with the positions of the additional changes indicated below the wild-type (WT) sequence. Amino acid positions and charged residues are indicated by numbers and plus/minus signs, respectively.

morphology, and growth characteristics similar to those of wild-type virus and no additional changes in the E, M, or N gene (Fig. 3). On the other hand, replacement of both negative charges with alanine residues gave rise to $DD_{440-441}$ viruses that retained the introduced substitutions but also had additional changes in which serine and arginine residues at positions 424 and 425 in the N protein were replaced by glycines (Fig. 3). These changes appeared quickly following electroporation, since relatively little cytopathic effect was observed during the first 24 h following electroporation, but a significant increase in fusion was present by 48 h. Sequence analysis prior to plaque purification indicated that the recovered virus consisted of a mixed population at positions 424 and 425 (data not shown). Seven plaques were selected and analyzed following five passages. All retained the original alanine substitutions and the additional glycine changes at positions 424 and 425. The plaque-purified viruses all exhibited plaque size, morphology, and growth kinetics indistinguishable from those of the wild-type virus (Fig. 3). Taken together, the data strongly indicate that negative charges are favored at positions 440 and 441, but they are not absolutely required. The results suggested that, even though neutral charges at these positions are tolerated, compensating changes appeared to be necessary for recovery of viable virus. The seemingly exponential growth of the $DD_{440-441}AA$ virus following electroporation suggested that there is strong selective pressure for the virus to compensate for the introduced changes.

Interestingly, unlike the double arginine substitution for the $DD_{440-441}$ residues, viruses were recovered with the substitution of a single positively charged arginine at either position. However, the $D_{440}R$ and $D_{441}R$ viruses exhibited a variety of genotypes (Fig. 4). All of the plaque-purified viruses for both the $D_{440}R$ and $D_{441}R$ viruses retained the introduced arginine, with one exception. One wild-type revertant was isolated from the $D_{441}R$ mutant. Approximately one-quarter of the analyzed plaques from the $D_{441}R$ mutant had no additional changes,

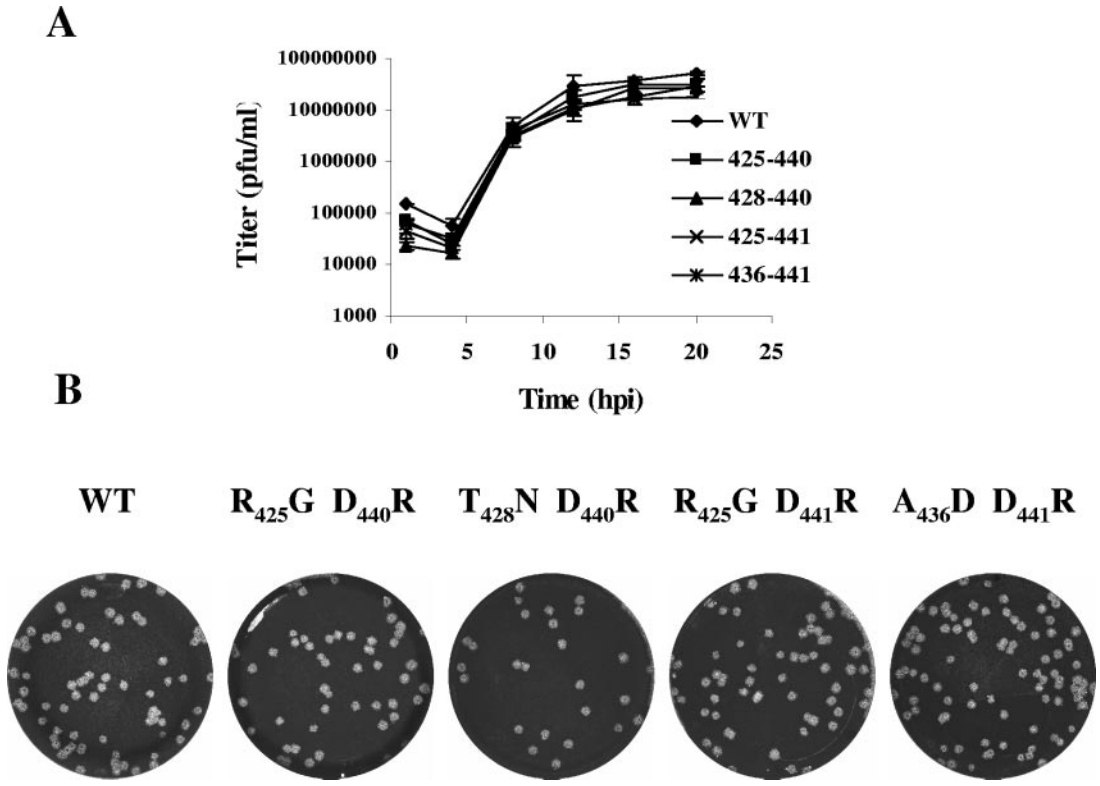

FIG. 5. Plaque morphologies and growth kinetics of reconstructed N mutant viruses with compensating changes. (A) Mouse 17Cl1 cells were infected with wild-type (WT) infectious cloned virus or $R_{425}G\ D_{440}R$, $T_{428}N\ D_{440}R$, $R_{425}G\ D_{441}R$, or $A_{436}D\ D_{441}R$ reconstructed virus at an MOI of 5. Growth kinetics properties were analyzed by plaque assay in L2 cells. The error bars indicate average deviations of two independent growth kinetics experiments. (B) Plaque sizes and morphologies of the compensated viruses relative to the wild-type virus in infected L2 cells are shown.

whereas all of the recovered $D_{440}R$ viruses exhibited additional changes in the N gene. The $D_{441}R$ viruses that exhibited no additional changes were genetically stable through five passages if allowed to grow for a short period, but the viruses were very crippled. They grew to titers 3 to 4 orders of magnitude lower than those of the wild-type parent and exhibited a small-plaque phenotype (Fig. 3).

The majority of the additional changes for both the $D_{440}R$ and $D_{441}R$ mutants were concentrated in the region between residues 424 and 436 in the N protein (Fig. 4). All of the recovered viruses with changes in this region exhibited wild-type phenotypes. Most of the recovered plaque-purified viruses for both mutants had an arginine-to-glycine change at position 425. The frequency of the changes strongly suggested that they might be compensating mutations that provided the mutant viruses with a significant growth advantage. Analysis showed that $D_{440}R$ plaques with either the $R_{425}G$ or the $T_{428}N$ change and $D_{441}R$ plaques with either the $R_{425}G$ or the $A_{436}D$ change were indistinguishable from wild-type virus in terms of plaque size, morphology, and growth characteristics.

Other changes within the N protein compensate for mutations in the $D_{440}R$ and $D_{441}R$ recovered viruses. To confirm which of the additional changes in the recovered viruses were providing a compensatory growth advantage, four independent viruses were constructed. We focused on the changes that were recovered most frequently, $R_{425}G$ coupled with $D_{440}R$ or $D_{441}R$, $T_{428}N$ in combination with $D_{440}R$, and $A_{436}D$ with $D_{441}R$ (Fig. 5). Each of the selected mutations was introduced, and new infectious clones were assembled to ensure that no other incidental changes elsewhere in the genome were providing a growth advantage to the virus.

Viruses were recovered from all of the newly constructed clones. The viruses were genetically stable, as demonstrated by sequence analysis of multiple independent plaques. The introduced amino acid substitutions were retained, and no other changes arose through the multiple passages. All four reconstructed mutant viruses displayed growth and plaque size/morphology indistinguishable from those of the wild-type virus (Fig. 5), thus confirming that the new changes most frequently present in the recovered viruses with the original mutations were indeed responsible for the growth advantage of the viruses.

Effects of the $D_{441}R$ mutation on viral protein and RNA levels. We were able to recover only a few $D_{441}R$ and no $D_{440}R$ mutant viruses that did not have additional compensating changes. The $D_{441}R$ virus was clearly crippled, since it exhibited a small-plaque phenotype (Fig. 3), slow growth, and very low titer. Working with the virus was difficult because of the low titer and the appearance of compensating changes that often arose when the virus was grown through multiple replication cycles. Nonetheless, we were able to carry out limited analysis of this virus, which provided some insight into how the mutant protein impacts virus growth. Initially, mouse L2 cells were infected at an MOI of 0.0001, and the amount of released

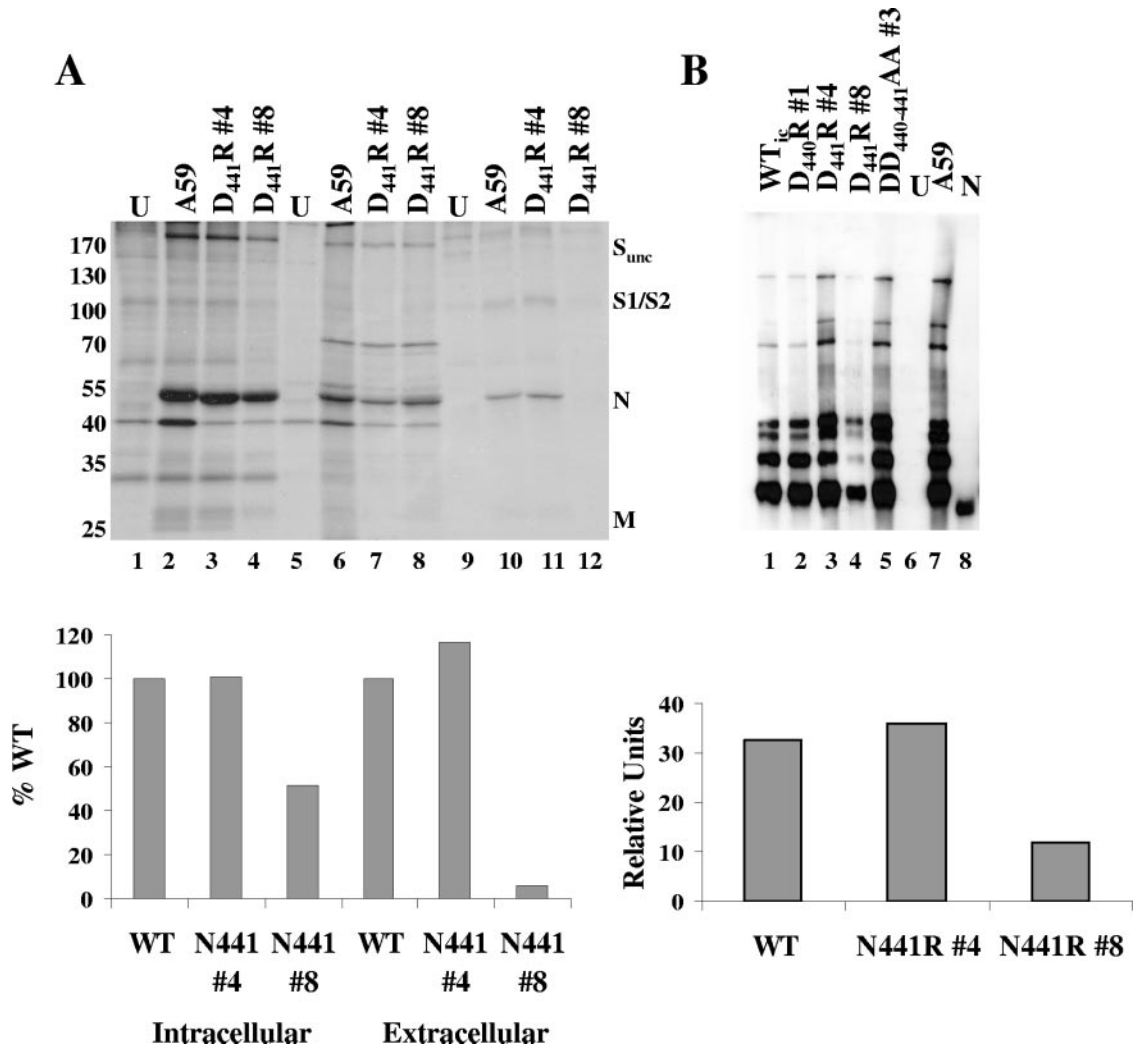

FIG. 6. Macromolecular synthesis of crippled $D_{441}R$ no. 8 compared with wild-type virus and recovered viruses with second-site compensating changes. Mouse 17Cl1 cells were infected at an MOI of 0.1. (A) Analysis of protein synthesis and extracellular virus. Proteins were metabolically radiolabeled with [^{35}S]methionine and cysteine for 30 min at 5 h p.i. (lanes 1 to 4) and chased for 4 h (lanes 5 to 12). Intracellular viral proteins (lanes 1 to 8) and extracellular virions (lanes 9 to 12) were immunoprecipitated and analyzed by SDS-PAGE and autoradiography (top). Molecular weights in thousands are show to the left, and the positions of the viral proteins are indicated on the right. Quantification of S, M, and N proteins was obtained by densitometry. The density values for intracellular viral proteins at 5.5 h p.i. were summed and are expressed relative to the same sum for the wild-type virus (bottom, Intracellular). Corresponding density values for the extracellular viruses at 9.5 h p.i. were normalized to the intracellular viral-protein sums at 5.5 h p.i. and plotted relative to the wild type (WT) (bottom, Extracellular). (B) Total intracellular RNA was extracted and analyzed by Northern blotting with a probe specific for the N gene (top). The numbers appended to the mutant names refer to specific plaque numbers of recovered viruses as described in the text. Density values for the sum of the four smallest subgenomic RNAs were expressed relative to the sum for the wild-type virus (bottom). Density values were obtained from Northern blot analysis similar to the one shown but exposed for a shorter time (bottom). The data represent average values from two experiments for both protein and RNA analyses.

virus was analyzed by plaque assay. No $N_{441}R$ mutant virus was detected at 11 h p.i., and 100 to 500 times less virus was detected during the 16- to 27-h p.i. period compared with the compensated $D_{441}R$ virus at these times (data not shown). The slow growth was consistent with the small-plaque phenotype and the slow expansion of the virus that were observed in the initial infections with the $N_{441}R$ mutant viruses that were recovered without any compensating changes.

To determine if the small plaque size and reduced growth correlated with the amount of viral macromolecular synthesis, viral protein and subgenomic RNA syntheses were examined. Mouse 17Cl1 cells were infected at an MOI of 0.1. Pulse-chase experiments revealed that at 5.5 h p.i., the overall viral protein synthesis for the $N_{441}R$ no. 8 mutant was approximately 50% of that observed with the wild-type virus and the recovered $N_{441}R$ no. 4 that contained the $R_{425}G$ compensating change. However, after a 4-h chase, the amount of extracellular $N_{441}R$ no. 8 virus was less than 10% of what was measured for the wild-type and $N_{441}R$ no. 4 viruses (Fig. 6A).

The viral RNA levels were also analyzed, since the N protein apparently plays some role in viral RNA synthesis (40). Cells were infected with wild-type virus and recovered viruses $D_{440}R$ no. 1, $D_{441}R$ no. 4, $D_{440\text{-}441}AA$ no. 3 (all with the compensatory glycines at positions 424 and/or 425), and $D_{441}R$ no. 8.

Intracellular RNA was harvested and analyzed by Northern blotting at 12 h p.i. using an N gene-specific probe. All of the recovered viruses, including the crippled $D_{441}R$ no. 8 virus, displayed the characteristic nested set of subgenomic RNAs (Fig. 6B). This indicated that the $D_{441}R$ no. 8 virus is transcriptionally functional, but the amount of intracellular subgenomic RNA was reduced by approximately one-third compared with the wild-type and $D_{441}R$ no. 4 viruses. In spite of the differences in subgenomic RNA amounts, we conclude, based on the level of protein synthesis and the virus output levels, that the mutant virus is not assembled as efficiently as the wild-type virus and compensated $D_{441}R$ no. 4 virus.

Mutations are predicted to impact the overall charge of domain III. A proteomics approach was taken to gain insight into how the various charge substitutions might impact the N protein. We used ScanSite pI/M_w, with the option to include phosphorylation sites, on the ExPASy proteomics server at the Swiss Institute of Bioinformatics to determine the predicted effect of the mutations and the compensating changes that were found in the recovered viruses on the theoretical pI of the N protein. The predicted pI for the wild-type protein is very basic, ranging between 9.76 for the unphosphorylated MHV-CoV A59 N protein and 9.38 if the protein is phosphorylated at as many as four sites. The individual changes that we introduced were predicted to result in small increases in the pI of the entire protein. If domain III and its concentration of conserved negative charges within the domain were functionally important for protein-proteins interactions, at least part of the domain would likely be exposed on the surface of the protein. We reasoned that analysis of this domain alone might provide insight into how our mutations could be disruptive and if the compensating changes that were observed would alleviate changes in the overall charge of the domain. Thus, we focused on domain III and its acidic subdomain, where the conserved negative charges are located (Table 2).

There is one predicted phosphorylation site at position T_{228} in domain III. Preliminary data in our laboratory suggested that the site is not phosphorylated on the virion-associated N, but we had not yet determined if the site is phosphorylated on the intracellular N protein (T. C. White and B. G. Hogue unpublished data). Therefore, we analyzed the domain both with and without phosphorylation of the site. Replacement of $DD_{440-441}$ with positive charges was predicted to have the greatest impact on the pI of domain III, with the most dramatic effect on its acidic domain (Table 2). In most cases an increase in the predicted pI correlated with a crippled phenotype of our mutant viruses, and the pI was predicted to be shifted back closer to that of the wild-type N in the mutants that were recovered with compensating changes. In the case of the $DD_{440-441}RR$ mutant, the pI for domain III was predicted to increase from 4.14 to 4.81 if T228 was not phosphorylated, whereas for its acidic subdomain, a change from 3.21 to 4.23 would result compared with the wild-type protein. In the most frequently recovered viruses with compensating changes, the overall charge of domain III was predicted to be less positive, closer to that of the wild-type protein. For example, the predicted pI of domain III of the $D_{441}R$ no. 4 virus would decrease to 4.24 compared with 4.42 for the $D_{441}R$ no. 8 virus, which lacked the $R_{425}G$ compensating change. This appears to be a relatively small change, but it is consistent with what was predicted for the viruses that were recovered with the introduced mutations at D_{446}, and singly within $EDD_{449-451}$, that had no other changes but grew like the wild type. The predictions are consistent with our conclusion that $DD_{440-441}$ are important in helping to maintain the overall negative charge of the domain.

TABLE 2. Predicted isoelectric points[a] of wild-type and mutant N protein domain III[b]

Virus	Domain III pI[c,d]	Acidic domain pI[e]	Recovered[d] domain III pI[g]
WT[f]	4.14, 3.99	3.21	
$D_{440}R$	4.42, 4.24	3.71	4.24 4.07 ($R_{425}G$ $D_{440}R$) 4.42 ($T_{428}N$ $D_{440}R$)
$D_{441}R$	4.42, 4.24	3.71	4.24 4.07 ($R_{425}G$ $D_{441}R$) 4.30 4.15 ($A_{436}D$ $D_{441}R$)
$DD_{440-441}RR$	4.81, 4.56	4.23	
$DD_{440-441}AA$	4.36, 4.17	3.37	4.16 3.97 ($SR_{424-425}GG$, $DD_{440-441}AA$)
$D_{440-441}EE$	4.22, 4.06	3.29	
$D_{446}A$	4.24, 4.07	3.28	
$D_{451}A$	4.24, 4.07	3.28	
$D_{451}E$	4.18, 4.02	3.25	
$EDD_{449-451}AAA$	4.46, 4.24	3.42	

[a] The isoelectric points are calculated using the algorithm from ExPASy's proteomics server at the Swiss Institute of Bioinformatics Compute pI/M_w program with the option to include phosphorylation sites.

[b] ^{406}EVDNVSVAKPKSSVQRNVSRELTPEDRSLLAQILDDGVVPDGLE DDSNV^{454}.

[c] Amino acids 406 to 454.

[d] Predicted pI values based on zero (left) or one (right) phosphorylation site at T228.

[e] Amino acids S433 to V454.

[f] WT, wild type.

[g] Wild-type amino acids and numbers, followed by the second-site amino acid changes ($R_{425}G$, $T_{428}N$, $R_{425}G$, $A_{436}D$, $SR_{424-425}GG$) or corresponding originally introduced mutations ($D_{440}R$, $D_{441}R$, $DD_{440-441}AA$) in recovered viruses are shown in parentheses.

DISCUSSION

In this study, we examined the importance of negatively charged amino acids located within the carboxy-terminal 22 amino acids of the MHV-CoV A59 N protein. We found that two of the residues, $DD_{440-441}$, are functionally important for virus output. When both of the aspartic acids were replaced by negatively charged glutamic acid residues, viruses with no new changes and a wild-type phenotype were recovered. Significantly, viruses were not recovered when both residues were replaced with positive charges. Replacement of both amino acids with neutrally charged alanine or individual replacement of either residue with positively charged arginine was tolerated, but the vast majority of the recovered viruses also had compensating changes which restored the wild-type phenotype. A few very crippled viruses were recovered that retained the single charge reversal substitution at position 441 without additional new changes. Altogether, the results indicate that the negative charges at positions 440 and 441 are key residues. The data support the idea that the residues are involved in virus assembly.

Maintenance of the overall negative charge within the carboxy end of the N protein appears to be important, since most of the compensating changes are predicted to impact the overall charge of the domain. The most prominent compensating change isolated was the replacement of R_{425} with glycine when

either D_{440} or D_{441} was changed to a positively charged residue. In addition to elimination of the positive charge at position 425, several recovered viruses from the $D_{441}R$ mutant had new changes in which amino acids were replaced by negative charges ($N_{422}D$ and $A_{436}D$). All of the recovered viruses with the $DD_{440\text{-}441}AA$ change had compensating changes, with S_{424} and R_{425} each replaced by glycine. Reconstruction of the N double mutants with both the original and new residues that were present in the recovered viruses confirmed that the additional changes provide a growth advantage. This was specifically illustrated with the few $D_{441}R$ mutants without compensating changes that were recovered, compared with the $D_{441}R$ recovered viruses that also had the $R_{425}G$ or $A_{436}D$ change that clearly suppressed the defect seen with the parental mutant virus. This apparent gain of function observed with the compensatory changes supports our conclusion that the overall balance of negative charges in this region is important for the function(s) of the protein. Furthermore, analysis of the predicted pI of domain III and its acidic domain for the wild type, mutants, and recovered compensated mutant viruses supports the conclusion. Replacement of $DD_{440\text{-}441}$ with positive charges had the greatest negative impact on the virus, since no viruses were recovered for this mutant. Replacement of these key residues, either singly or together, is predicted to result in an increase in the pI of domain III and, more dramatically, its acidic domain. In the most frequently recovered viruses with compensating changes, the overall charge of domain III is predicted to be less positive, closer to that of the wild-type protein. This is consistent with our conclusion that $DD_{440\text{-}441}$ are important in helping to maintain the overall negative charge of the domain.

There are several possibilities that may account for the importance of the negative charges in domain III of the multifunctional N protein. Data from both biochemical and genetic analyses have clearly established that the M protein interacts with viral nucleocapsids (13, 22, 29). A number of other potential functions are more speculative or less well defined. N protein molecules likely interact with each other in the helical nucleocapsid structure. There seems to be some variation among coronaviruses, but N molecules are thought to homo-oligomerize. MHV-CoV N is thought to form trimers, whereas recent data on SARS-CoV suggest that N forms dimers and tetramers (18, 28, 38a, 51). Recently, evidence for a role of the N protein in viral transcription and/or replication was provided (40). It has also been suggested that SARS N may impact cell signaling pathways (17). Since charged residues often mediate protein-protein interactions, the conserved negative charges may participate in important specific N-protein (N-M and N-N, other N-virus, or N-host) interactions that are involved in any of the roles that N plays during the virus life cycle. The $DD_{440\text{-}441}$ residues conceivably could participate in electrostatic interactions involved in any of these functions.

While the reviews of our work were being addressed, results from a study similar to ours were published (20). A series of clustered charge-to-alanine mutations were introduced by targeted RNA recombination into the carboxy end of the MHV-CoV N protein in the study. Aspartic acids 440 and 441 were also identified in the study as important key residues in the protein. Interestingly, viruses were recovered with compensating changes not only in the N gene, as we found, but also within the M gene. Roughly one-third of the recovered viruses had compensating changes in M. As with our study, compensating changes in the N gene mapped within domain III. The major compensating change within N was replacement of glutamine 437 by leucine. This change would not result in a difference in the overall charge of the domain compared with the parental $DD_{440\text{-}441}AA$ mutant. It was hypothesized that the $Q_{437}L$ substitution might result in replacement of a lost electrostatic interaction with a hydrophobic interaction between the carboxy ends of the N and M proteins. Evidence from the study strongly suggests that D_{440} and D_{441} are involved in mediating N-M interactions during virus assembly. Overall, the results of that study and ours are complementary, since both independently identified the same key residues using different reverse-genetic approaches. Each study also provides unique additional new information that reveals new insights into an obviously important functional domain in the multifunctional N protein.

We entered our study with the assumption that electrostatic charge interactions likely occur between the carboxy ends of the N and M proteins during virus assembly. This assumption was based in part on the results of an earlier study in which deletion of the penultimate positive charge at the COOH end of the MHV M protein resulted in recovery of viruses with additional changes in both the M and N proteins that could compensate for the charge loss (22). We expected that if any of our charge substitution mutations impacted the M-nucleocapsid interaction, and if the compensatory changes could restore the function, some of the additional changes would map within the M protein. It is clear from the recently published study by Hurst et al. that changes within M can compensate for $DD_{440\text{-}441}$ mutations. It is not clear why all of the compensating changes that we identified mapped within the N gene and why a greater number of compensatory changes were identified. Nonetheless, our results strongly demonstrate that the loss of the negative charges at amino acid positions 440 and 441 can be compensated for by several changes that map within 15 to 20 residues amino terminal to the residues in the N protein alone. Our compensating changes in N arose quickly following electroporation of the full-length infectious cloned RNA, indicating that removal of the negative charges places significant pressure on the virus for selection of more fit, viable viruses. Once the new changes arose within N, the virus was apparently no longer under pressure for additional changes to arise elsewhere within the genome that might alternatively compensate for the lethal or crippling effects of the charge reversals at positions 440 and 441.

Our $DD_{440\text{-}441}$ charge substitution mutants clearly had an impact on virus growth and output. Replacement of both residues with positive charges was apparently lethal to the virus, since we were not able to recover virus following electroporation. The few $D_{441}R$ viruses that were isolated with only the introduced single substitution all exhibited a very crippled phenotype, giving rise to very small plaques and titers that were significantly below that of the wild-type virus. This reduction is less than what would be expected based on the amount of intracellular viral protein synthesized by the mutant. This strongly indicates that virus assembly is compromised when the negatively charged $DD_{440\text{-}441}$ residues are removed.

Further studies will be necessary to determine whether the

$DD_{440-441}$ residues are involved in transcription and/or replication in addition to virus assembly. The reduction in $D_{441}R$ virus output compared with the wild type and the compensated parent virus could account for the reduced total viral subgenomic RNA of the mutant. However, we cannot exclude at this point the possibility that the $D_{441}R$ mutation has a direct effect on whatever role N plays in viral RNA synthesis. There is precedent for a multifunctional role of the nucleocapsid proteins of other viruses. The N proteins of negative-stranded RNA viruses, in addition to functioning as structural components, are also thought to play roles in transcription, replication, and intracellular trafficking of viral genomes. For example, the N protein of vesicular stomatitis virus encapsidates the genomic RNA as a helical ribonucleoprotein structure, but it has also been demonstrated in many studies that the protein is involved in RNA replication (47). A new model for vesicular stomatitis virus transcription and replication was recently described in which the RNA polymerase exists as part of two distinct complexes in virus-infected cells (38). The transcriptase complex consists of the polymerase (L), phosphoprotein (P), and host proteins, while the replicase complex consists of the L, P, and N proteins. The N protein also obviously functions as a structural component of virions, since it encapsidates the genomic RNA. The influenza nucleoprotein is another example of a structural protein that encapsidates the virus genome. Results from many studies suggest that the NP protein is also involved viral RNA synthesis as part of the ribonucleoprotein particle (37). How easy it will be to uncouple virus assembly and RNA synthesis in coronavirus-infected cells remains to be determined.

The concentration of primarily negative charges in domain III of coronavirus N proteins is a conserved feature across the family. However, the inability of the domains to be exchanged between two closely related group II coronaviruses suggests that more than just the charged residues are important (36). Since we identified compensating changes only within the N protein itself, this suggests that, in addition to maintaining the net negative charge, the overall structure of the carboxy-terminal region of the protein may be important in allowing the protein, more specifically domain III, to play its functional role(s) in N-N, N-M, or other N-protein interactions. The frequency with which R_{425} was replaced with glycine when the single positive charges were introduced at position 440 or 441, as well as the additional replacement of the adjacent amino acid 424 in the case where both were mutated, is consistent with the idea that the structural presentation of the negative charges is likely important. The small side chain on glycine promotes conformational freedom and allows greater flexibility in the surrounding areas, especially when multiple glycines are in close proximity to each other (32). Since structural information on the N protein is limited, definitive assessment of the importance and requirements for presentation of the negative charges in the context of the whole molecule must await the availability of this information. A series of protease digestions and mass spectrometry identification of peptides released over a time course suggest that the acidic domain is exposed on the surface (White and Hogue, unpublished). Recently, the three-dimensional structures of the N termini of both SARS-CoV N (residues 45 to 181) and infectious bronchitis virus N (residues 29 to 160) were determined by nuclear magnetic resonance and crystallization, respectively (14, 19). In the case of IBV N, it was proposed that the carboxy end, but not including the extreme end of the domain, where negatively charged residues are concentrated, is important for oligomerization of the protein (14). Clearly, further structural studies are important to better define the conformational and dynamic changes within the carboxy-terminal negatively charged domain of this important multifunctional protein that are responsible for helping to drive virion assembly and the possible involvement in other N-protein interactions involved in the other functional roles of the protein.

ACKNOWLEDGMENTS

This work was supported by Public Health Service grant AI53704 from the National Institute of Allergy and Infectious Diseases to B.G.H. and a grant from the Biological Research Experience for Undergraduates (BREU) at ASU to V.B. and A.B.

We are grateful to Ralph Baric for providing the MHV-CoV A59 infectious clone and BHK-MHVR cells and to Kathryn Holmes for the F88 antibody. We thank members of the Hogue laboratory for helpful discussions and comments throughout the study.

REFERENCES

1. **Almazan, F., C. Galan, and L. Enjuanes.** 2004. The nucleoprotein is required for efficient coronavirus genome replication. J. Virol. **78:**12683–12688.
2. **Baric, R. S., G. W. Nelson, J. O. Fleming, R. J. Deans, J. G. Keck, N. Casteel, and S. A. Stohlman.** 1988. Interactions between coronavirus nucleocapsid protein and viral RNAs: implications for viral transcription. J. Virol. **62:** 4280–4287.
3. **Bos, E. C., W. Luytjes, H. V. van der Meulen, H. K. Koerten, and W. J. Spaan.** 1996. The production of recombinant infectious DI-particles of a murine coronavirus in the absence of helper virus. Virology **218:**52–60.
4. **Casais, R., V. Thiel, S. G. Siddell, D. Cavanagh, and P. Britton.** 2001. Reverse genetics system for the avian coronavirus infectious bronchitis virus. J. Virol. **75:**12359–12369.
5. **Chang, R. Y., and D. A. Brian.** 1996. *cis* Requirement for N-specific protein sequence in bovine coronavirus defective interfering RNA replication. J. Virol. **70:**2201–2207.
6. **Cologna, R., J. F. Spagnolo, and B. G. Hogue.** 2000. Identification of nucleocapsid binding sites within coronavirus-defective genomes. Virology **277:** 235–249.
7. **Compton, S. R., D. B. Rogers, K. V. Holmes, D. Fertsch, J. Remenick, and J. J. McGowan.** 1987. In vitro replication of mouse hepatitis virus strain A59. J. Virol. **61:**1814–1820.
8. **Corse, E., and C. E. Machamer.** 2000. Infectious bronchitis virus E protein is targeted to the Golgi complex and directs release of virus-like particles. J. Virol. **74:**4319–4326.
9. **Curtis, K. M., B. Yount, and R. S. Baric.** 2002. Heterologous gene expression from transmissible gastroenteritis virus replicon particles. J. Virol. **76:**1422–1434.
10. **Davies, H. A., R. R. Dourmashkin, and M. R. Macnaughton.** 1981. Ribonucleoprotein of avian infectious bronchitis virus. J Gen. Virol. **53:**67–74.
11. **de Haan, C. A., H. Vennema, and P. J. Rottier.** 2000. Assembly of the coronavirus envelope: homotypic interactions between the M proteins. J. Virol. **74:**4967–4978.
12. **Denison, M. R., W. J. Spaan, Y. van der Meer, C. A. Gibson, A. C. Sims, E. Prentice, and X. T. Lu.** 1999. The putative helicase of the coronavirus mouse hepatitis virus is processed from the replicase gene polyprotein and localizes in complexes that are active in viral RNA synthesis. J. Virol. **73:**6862–6871.
13. **Escors, D., J. Ortego, H. Laude, and L. Enjuanes.** 2001. The membrane M protein carboxy terminus binds to transmissible gastroenteritis coronavirus core and contributes to core stability. J. Virol. **75:**1312–1324.
14. **Fan, H., A. Ooi, Y. W. Tan, S. Wang, S. Fang, D. X. Liu, and J. Lescar.** 2005. The nucleocapsid protein of coronavirus infectious bronchitis virus: crystal structure of its N-terminal domain and multimerization properties. Structure **13:**1859–1868.
15. **Gallagher, T. M., and M. J. Buchmeier.** 2001. Coronavirus spike proteins in viral entry and pathogenesis. Virology **279:**371–374.
16. **Gasteiger, E., A. Gattiker, C. Hoogland, I. Ivanyi, R. D. Appel, and A. Bairoch.** 2003. ExPASy: the proteomics server for in-depth protein knowledge and analysis. Nucleic Acids Res. **31:**3784–3788.
17. **He, R., A. Leeson, A. Andonov, Y. Li, N. Bastien, J. Cao, C. Osiowy, F. Dobie, T. Cutts, M. Ballantine, and X. Li.** 2003. Activation of AP-1 signal transduction pathway by SARS coronavirus nucleocapsid protein. Biochem. Biophys. Res. Commun. **311:**870–876.

18. **Hogue, B. G., B. King, and D. A. Brian.** 1984. Antigenic relationships among proteins of bovine coronavirus, human respiratory coronavirus OC43, and mouse hepatitis coronavirus A59. J. Virol. **51:**384–388.
19. **Huang, Q., L. Yu, A. M. Petros, A. Gunasekera, Z. Liu, N. Xu, P. Hajduk, J. Mack, S. W. Fesik, and E. T. Olejniczak.** 2004. Structure of the N-terminal RNA-binding domain of the SARS CoV nucleocapsid protein. Biochemistry **43:**6059–6063.
20. **Hurst, K. R., L. Kuo, C. A. Koetzner, R. Ye, B. Hsue, and P. S. Masters.** 2005. A major determinant for membrane protein interaction localizes to the carboxy-terminal domain of the mouse coronavirus nucleocapsid protein. J. Virol. **79:**13285–13297.
21. **Klumperman, J., J. K. Locker, A. Meijer, M. C. Horzinek, H. J. Geuze, and P. J. Rottier.** 1994. Coronavirus M proteins accumulate in the Golgi complex beyond the site of virion budding. J. Virol. **68:**6523–6534.
22. **Kuo, L., and P. S. Masters.** 2002. Genetic evidence for a structural interaction between the carboxy termini of the membrane and nucleocapsid proteins of mouse hepatitis virus. J. Virol. **76:**4987–4999.
23. **Kuo, L., and P. S. Masters.** 2003. The small envelope protein E is not essential for murine coronavirus replication. J. Virol. **77:**4597–4608.
24. **Laude, H., and P. S. Masters.** 1995. The coronavirus nucleocapsid protein, p. 141–163. *In* S. G. Siddell (ed.), The Coronaviridae. Plenum, New York, N.Y.
25. **Liao, Y., J. Lescar, J. P. Tam, and D. X. Liu.** 2004. Expression of SARS-coronavirus envelope protein in *Escherichia coli* cells alters membrane permeability. Biochem. Biophys. Res. Commun. **325:**374–380.
26. **Macneughton, M. R., and H. A. Davies.** 1978. Ribonucleoprotein-like structures from coronavirus particles. J. Gen. Virol. **39:**545–549.
27. **Madan, V., M. J. Garcia, M. A. Sanz, and L. Carrasco.** 2005. Viroporin activity of murine hepatitis virus E protein. FEBS Lett. **579:**3607–3612.
28. **Narayanan, K., K. H. Kim, and S. Makino.** 2003. Characterization of N protein self-association in coronavirus ribonucleoprotein complexes. Virus Res. **98:**131–140.
29. **Narayanan, K., A. Maeda, J. Maeda, and S. Makino.** 2000. Characterization of the coronavirus M protein and nucleocapsid interaction in infected cells. J. Virol. **74:**8127–8134.
30. **Narayanan, K., and S. Makino.** 2001. Characterization of nucleocapsid-M protein interaction in murine coronavirus. Adv. Exp. Med. Biol. **494:**577–582.
31. **Nguyen, V. P., and B. G. Hogue.** 1997. Protein interactions during coronavirus assembly. J. Virol. **71:**9278–9284.
32. **Oh, D., S. Y. Shin, S. Lee, J. H. Kang, S. D. Kim, P. D. Ryu, K. S. Hahm, and Y. Kim.** 2000. Role of the hinge region and the tryptophan residue in the synthetic antimicrobial peptides, cecropin A(1-8)-magainin 2(1-12) and its analogues, on their antibiotic activities and structures. Biochemistry **39:** 11855–11864.
33. **Opstelten, D. J., M. J. Raamsman, K. Wolfs, M. C. Horzinek, and P. J. Rottier.** 1995. Envelope glycoprotein interactions in coronavirus assembly. J. Cell Biol. **131:**339–349.
34. **Ortego, J., D. Escors, H. Laude, and L. Enjuanes.** 2002. Generation of a replication-competent, propagation-deficient virus vector based on the transmissible gastroenteritis coronavirus genome. J. Virol. **76:**11518–11529.
35. **Parker, M. M., and P. S. Masters.** 1990. Sequence comparison of the N genes of five strains of the coronavirus mouse hepatitis virus suggests a three domain structure for the nucleocapsid protein. Virology **179:**463–468.
36. **Peng, D., C. A. Koetzner, T. McMahon, Y. Zhu, and P. S. Masters.** 1995. Construction of murine coronavirus mutants containing interspecies chimeric nucleocapsid proteins. J. Virol. **69:**5475–5484.
37. **Portela, A., and P. Digard.** 2002. The influenza virus nucleoprotein: a multifunctional RNA-binding protein pivotal to virus replication. J. Gen. Virol. **83:**723–734.
38. **Qanungo, K. R., D. Shaji, M. Mathur, and A. K. Banerjee.** 2004. Two RNA polymerase complexes from vesicular stomatitis virus-infected cells that carry out transcription and replication of genome RNA. Proc. Natl. Acad. Sci. USA **101:**5952–5957.

38a. **Robbins, S. G., M. F. Frana, J. J. McGowan, J. F. Boyle, and K. V. Holmes.** 1986. RNA-binding proteins of coronavirus MHV: detection of multimeric N protein with an RNA overlay-protein blot assay.Virology **150:**402–410.

39. **Sawicki, S. G., and D. L. Sawicki.** 2005. Coronavirus transcription: a perspective. Curr. Top. Microbiol. Immunol. **287:**31–55.
40. **Schelle, B., N. Karl, B. Ludewig, S. G. Siddell, and V. Thiel.** 2005. Selective replication of coronavirus genomes that express nucleocapsid protein. J. Virol. **79:**6620–6630.
41. **Spagnolo, J. F., and B. G. Hogue.** 2000. Host protein interactions with the 3′ end of bovine coronavirus RNA and the requirement of the poly(A) tail for coronavirus defective genome replication. J. Virol. **74:**5053–5065.
42. **Tahara, S. M., T. A. Dietlin, C. C. Bergmann, G. W. Nelson, S. Kyuwa, R. P. Anthony, and S. A. Stohlman.** 1994. Coronavirus translational regulation: leader affects mRNA efficiency. Virology **202:**621–630.
43. **Thompson, J. D., D. G. Higgins, and T. J. Gibson.** 1994. CLUSTAL W: improving the sensitivity of progressive multiple sequence alignment through sequence weighting, position-specific gap penalties and weight matrix choice. Nucleic Acids Res. **22:**4673–4680.
44. **Tooze, J., S. Tooze, and G. Warren.** 1984. Replication of coronavirus MHV-A59 in sac$^-$ cells: determination of the first site of budding of progeny virions. Eur. J. Cell Biol. **33:**281–293.
45. **van der Meer, Y., E. J. Snijder, J. C. Dobbe, S. Schleich, M. R. Denison, W. J. Spaan, and J. K. Locker.** 1999. Localization of mouse hepatitis virus nonstructural proteins and RNA synthesis indicates a role for late endosomes in viral replication. J. Virol. **73:**7641–7657.
46. **Vennema, H., G. J. Godeke, J. W. Rossen, W. F. Voorhout, M. C. Horzinek, D. J. Opstelten, and P. J. Rottier.** 1996. Nucleocapsid-independent assembly of coronavirus-like particles by co-expression of viral envelope protein genes. EMBO J. **15:**2020–2028.
47. **Whelan, S. P., J. N. Barr, and G. W. Wertz.** 2004. Transcription and replication of nonsegmented negative-strand RNA viruses. Curr. Top. Microbiol. Immunol. **283:**61–119.
48. **Wilson, L., C. McKinlay, P. Gage, and G. Ewart.** 2004. SARS coronavirus E protein forms cation-selective ion channels. Virology **330:**322–331.
49. **Yount, B., K. M. Curtis, and R. S. Baric.** 2000. Strategy for systematic assembly of large RNA and DNA genomes: transmissible gastroenteritis virus model. J. Virol. **74:**10600–10611.
50. **Yount, B., M. R. Denison, S. R. Weiss, and R. S. Baric.** 2002. Systematic assembly of a full-length infectious cDNA of mouse hepatitis virus strain A59. J. Virol. **76:**11065–11078.
51. **Yu, I. M., C. L. Gustafson, J. Diao, J. W. Burgner, Z. Li, J. Zhang, and J. Chen.** 2005. Recombinant severe acute respiratory syndrome (SARS) coronavirus nucleocapsid protein forms a dimer through its C-terminal domain. J. Biol. Chem. **280:**23280–23286.